Austenite formation in 0.2% C and 0.45% C steels under conventional and ultrafast heating

Castro Cerda, F. M.; Sabirov, I.; Goulas, Konstantinos; Sietsma, J.; Monsalve, A.; Petrov, R. H.

DOI
10.1016/j.matdes.2016.12.009

Publication date
2017

Document Version
Final published version

Published in
Materials & Design

Citation (APA)
Castro Cerda, F. M., Sabirov, I., Goulas, K., Sietsma, J., Monsalve, A., & Petrov, R. H. (2017). Austenite formation in 0.2% C and 0.45% C steels under conventional and ultrafast heating. *Materials & Design*, *116*, 448-460. https://doi.org/10.1016/j.matdes.2016.12.009

Materials and Design 116 (2017) 448–460

Contents lists available at ScienceDirect

Materials and Design

journal homepage: www.elsevier.com/locate/matdes

Austenite formation in 0.2% C and 0.45% C steels under conventional and ultrafast heating

F.M. Castro Cerda [a,b,*], I. Sabirov [c], C. Goulas [d,e], J. Sietsma [a,d], A. Monsalve [b], R.H. Petrov [a,d]

[a] Department of Materials Science and Engineering, Ghent University, Technologiepark 903, 9052 Gent, Belgium
[b] Department of Metallurgical Engineering, Universidad de Santiago de Chile, Av. Lib. Bdo. O'Higgins 3363, Estación Central, Santiago de Chile, Chile
[c] IMDEA Materials Institute, Calle Eric Kandel 2, Getafe, 28906 Madrid, Spain
[d] Delft University of Technology, Department of Materials Science and Engineering, Mekelweg 2, 2628CD Delft, The Netherlands
[e] Materials innovation institute (M2i), Electronicaweg 25, 2628 XD Delft, The Netherlands

HIGHLIGHTS

- In ferrite-pearlite microstructures at conventional heating rates, the austenite formation is controlled by carbon diffusion
- At ultrafast heating rates, there is a transition in the mechanism of austenite formation from diffusion control to massive
- The transition temperature from carbon diffusion controlled to massive is thermodynamically defined for the first time
- Novel experimental evidence of austenite nucleation and growth mechanisms is provided

GRAPHICAL ABSTRACT

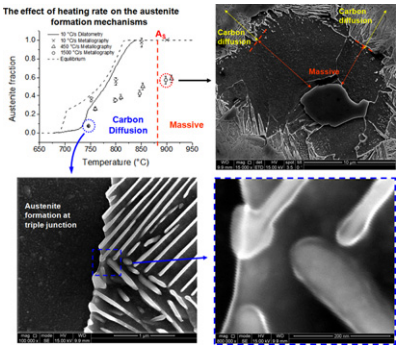

ARTICLE INFO

Article history:
Received 26 September 2016
Received in revised form 21 November 2016
Accepted 2 December 2016
Available online 6 December 2016

Keywords:
Austenite
Ultrafast heating
Thermodynamics
Kinetics
Steel
Phase transformation

ABSTRACT

The austenite formation in 0.2% C and 0.45% C steels with the initial microstructure of ferrite and pearlite has been studied. The effect of conventional (10 °C/s), fast (50 °C/s–100 °C/s) and ultrafast heating rates (>100 °C/s) on the austenite nucleation and growth mechanisms is rationalized. Scanning Electron Microscopy (SEM), and Electron BackScatter Diffraction (EBSD) analyses provide novel experimental evidence of the austenite nucleation and growth mechanisms operating at ultrafast heating rates. Two mechanisms of austenite formation are identified: diffusional and massive. It is demonstrated that at conventional heating rates the austenite formation kinetics are determined by carbon diffusion, whereas at ultrafast heating rates formation of austenite starts by carbon diffusion control, which is later overtaken by a massive mechanism. Comprehensive thermodynamic and kinetic descriptions of austenite nucleation and growth are developed based on experimental results.

1. Introduction

The ferrite-pearlite microstructure is the most produced microstructure in low and medium carbon steels and hence it follows as the most appropriate microstructure for the study of austenite formation. Some

* Corresponding author at: Department of Materials Science and Engineering, Ghent University, Technologiepark 903, 9052 Gent, Belgium.
E-mail address: felipemanuel.castrocerda@ugent.be (F.M. Castro Cerda).

http://dx.doi.org/10.1016/j.matdes.2016.12.009
0264-1275/

pioneering studies [1–3] have clarified many important aspects of the isothermal formation of austenite from pearlite, which were further extended to the study of austenite formation in ferrite-pearlite aggregates [4]. Nevertheless, it was also realized early on that the formation of austenite is a structure-sensitive process, and thus the initial microstructure plays an important role in the austenite formation process and the morphology of formed austenite. On that matter, considerable work on the formation of austenite was done on pure iron [2,5] and on steels with initial microstructure of ferrite and spheroidized cementite [6]. Other early studies have included martensite [7], bainite and mixtures of these constituents as starting microstructures for the isothermal formation of austenite. The main characteristics of austenite formation starting from ferrite-pearlite aggregates were first summarized in the metallographic work performed by Mehl in 1941 [1]. The key findings reported therein can be summarized as: (i) the austenite formation is a thermally activated process, (ii) nucleation of austenite occurs at pearlite boundaries, (iii) formation of carbon gradients takes place during austenite growth, (iv) the time for the complete formation of austenite decreases as the pearlitic interlamellar spacing decreases and it is only weakly dependent on the size of the colony, (v) cementite dissolution has much slower dissolution kinetics than ferrite. Subsequent studies have confirmed the conclusions above [2,3], and have served as a basis for the development of diffusional models describing austenite formation. However, most of the available kinetic descriptions of austenite formation are based upon isothermal conditions [4,8–16] and not on heating experiments.

Some of the key theoretical aspects of ultrafast heating of carbon steels were recently summarized by Meshkov and Pereloma [17]. Among the most important ones are: (i) there is an influence of the initial microstructure on the mechanism of formation of austenite (which was reported earlier by Gridnev and Trefilov in 1954 [7]), (ii) the nucleation stage can either be accomplished by diffusional or diffusionless mechanisms and (iii) growth stage can be diffusion controlled or interface controlled (massive). Regarding (ii), Kaluba et al. [18] have initiated an interesting debate [19–21] by claiming a novel 'bainitic transformation' mechanism for the austenite formation when ultrafast heating rates are applied. This mechanism assumes formation of austenite sheaves at grain boundaries and their further growth into grain interior, similar to the case of bainitic transformation. Aaronson and Nie [19] questioned these interpretations and proposed alternative ones based on existing mechanisms of bainitic transformation. Later, Hillert [20] proposed another explanation of Kaluba's observations relating them to the formation of Widmanstätten ferrite. About (iii), experimental evidence of massive transformation in medium carbon steels has been provided in the literature [22,23], even for heating rates as low as 1 °C/s.

There have been many attempts to model the anisothermal austenite formation starting from ferrite-pearlite microstructures [22,24–26]. The data collection in most of the studies stems from dilatometric experiments, where heating rates are limited to the range of 0.01–20 °C/s. In some other cases, the experiments consider heating rates up to 300 °C/s [25]. The highest heating rate employed in a 1D simulation of austenite growth is 1000 °C/s [26], although the simulations only considered the growth of austenite controlled by carbon diffusion, and were not compared to any experimental data. A complete treatment of the austenite formation, including the transition from a diffusion-controlled to an interface-controlled mechanism on heating, is described in [24]. However, neither a clear thermodynamic definition of the transition temperature (termed as $T_{massive}$) or experimental evidence supporting the change in the mechanism of austenite formation during heating is provided. Schmidt et al. [22] performed in-situ observations of austenite formation on heating. They suggested T_0 as the temperature for the change in the mechanism of austenite formation from diffusion controlled to interface controlled. Despite the lack of agreement on the definition of the temperature for the transition of the austenite formation mechanism, the main features of austenite formation reported in later studies are in strong agreement with [1]. The formation of austenite during heating consists of the simultaneous transformations of (a) pearlite → austenite and (b) ferrite → austenite. Some authors considered the formation of austenite as a two-stage process, in which transformation (b) occurs only after (a) [25,26]. The latter is a simplification of the actual situation described for the formation of austenite, which probably stems from the remarkable difference between the kinetics of pearlite and ferrite transformations [27]. A gradual change in the kinetics of ferrite transformation (b) during heating is also expected above a certain thermodynamic threshold, and experimental data have also been reported in [22] supporting this claim. The change in kinetics is in essence due to the change from carbon diffusion control to interface mobility control. However, the shift in the phase transformation mechanism is only noticeable above certain heating rates. Ultrafast heating (UFH) experiments provide the ideal conditions to study the kinetic transition from carbon diffusion control to interface mobility control of the austenite formation, as well as the microstructural features of austenite nucleation and growth at the very early stages of its formation. The main objective of the present work is to gain a fundamental understanding of the effect of heating rate and carbon content on the mechanisms of austenite nucleation and growth by a combination of experimental and theoretical techniques. In-depth microstructural characterization and the quantification of the transition temperature for diffusion controlled to massive formation of austenite are developed in this study. The results are expected to be of significance for the understanding of the effect of ultrafast heating on the formation of austenite in low-carbon ferrite-pearlite aggregates.

2. Experimental

2.1. Material and experiments

Heating experiments were carried out on two different steel grades, namely 0.2% C and 0.45% C in the hot rolled condition. The chemical composition of both steels is shown in Table 1. Two kinds of heating tests at different heating rates were performed: 1) heating to 100% austenite formation, 2) peak-annealing tests followed by quenching, resulting in partial austenite formation. In the first type of testing, the specimen was heated at a constant heating rate up to a certain temperature in the fully austenitic range, whereas in the latter type of test, the specimen was quenched after reaching a certain temperature between the onset and finishing of austenite formation. Heating to complete austenitization experiments were run in a DIL805bD Bähr Dilatometer for heating rates up to 200 °C/s, and the peak annealing tests in a Gleeble 3800 thermomechanical simulator for heating rates of 10 °C/s, 450 °C/s and 1500 °C/s. Gleeble test specimens were subjected to peak annealing experiments at 750 °C, 800 °C, 850 °C, 900 °C and 1100 °C with holding times < 0.1 s. Cooling (quenching) rates were ~− 160 °C/s for dilatometry and ~− 2000 °C/s for Gleeble experiments. Rectangular specimens of $10 \times 5 \times 1$ mm^3 were used for dilatometry and cylindrical specimens of 6 mm diameter and 116 mm length, threaded at both ends, were machined for Gleeble tests. The axis of both types of samples was along the rolling direction (RD). In both cases, a thin wire thermocouple (S-type) was spot welded to the midsection of each specimen to control the temperature during annealing. Another S-type thermocouple was welded at the distance of 3 mm from the midsection to measure the temperature gradient during the experiments.

Table 1
Chemical composition (in wt.%) of studied steels.

Steel	C	Mn	Si	Cu	Fe
0.2% C	0.17	1.08	0.22	0.27	Bal.
0.45% C	0.44	0.63	0.26	0.23	Bal.

2.2. Characterization and data analysis

The microstructure evolution was studied by Optical Microscopy (OM), Scanning Electron Microscopy (SEM), and Electron Backscattered Diffraction (EBSD). To avoid any effect of temperature gradients along the sample length (i.e. along RD), metallographic specimens were cut from the middle section of each test sample. The characterization was thus performed on the rolling plane at the center of the heat-treated sample, where the thermocouple was placed. The metallographic samples were prepared according to the standard procedure by grinding and polishing to 1 μm diamond paste. The microstructure was revealed by etching with a solution of 4% HNO_3 in ethanol (Nital 4%) for ~10 s at room temperature. Electron BackScatter Diffraction (EBSD) analysis was performed using a FEI Quanta™ 450-FEG-SEM operated at 20 kV, beam current corresponding to FEI spot size 5 for aperture 30 μm and working distance of 16 mm. The samples were 70° tilted towards the EBSD detector, and the EBSD patterns were acquired with a Hikari detector operated with EDAX-TSL-OIM-Data Collection version 6 software in a hexagonal scan grid. The orientation data were post-processed using the following grain definition: grain boundary misorientation higher than 5°, minimum 4 pixels per grain and a confidence index (CI) larger than 0.1.

The phase fraction during the anisothermal dilatometric heat treatment is commonly approximated using the lever rule. Such an approach, however, produces significant deviations, which can be some tens of percents, from actual values because of the density difference between pearlite and ferrite [25,28,29]. In the present study, the correction proposed in [28] is accepted and shall be used to calculate the austenite phase fractions from dilatometric data. The phase fractions measured from OM (cf. Table 4) were estimated from the area fraction of each microstructural constituent. The measurements of area fraction were performed using the software ImageJ. The volume fraction of austenite (martensite) estimated from EBSD measurements (cf. Fig. 3) was carried out using the Grain Average Image Quality (GAIQ) criteria described elsewhere [30].

Thermodynamic calculations were performed using the software ThermoCalc, database TCFE7. The critical temperatures for both materials are shown in Table 2. A_M has been defined as the temperature above which the free energy of austenite is lower than the free energy of ferrite when the carbon content approaches zero. Simulations of the microstructure during heating at different heating rates were carried out to study the movement of the γ/α interface in proeutectoid ferrite. The simulations were performed using the Dictra software, which allows the computation of diffusion-controlled transformation kinetics in multicomponent metallic systems. The general description of the software and the model can be found elsewhere [31–33]. The microstructure was simulated assuming an initial spherical representative volume and phase distribution as indicated in Fig. 1. The dimensions (R_1 is the radius of the pearlite colony and R_2 is the difference between the total radius and the radius of the pearlitic colony) and relative fractions (f_P is the volume fraction of pearlite) of each phase and their chemical composition were calculated keeping the mass balanced in the initial material, and these parameters are provided in Table 3. Three heating rates were simulated: 10 °C/s, 450 °C/s and 1500 °C/s. It was assumed that all pearlite was quickly transformed into austenite when the system reached the α + γ equilibrium range. As shown in Section 3, this assumption is consistent with the results of dilatometric and metallographic analysis. The initial chemical composition of each phase was estimated with ThermoCalc at a temperature in the range of ferrite and cementite metastable equilibrium. Calculated volumetric phase fractions were estimated neglecting the effect of carbon on the phase density.

Table 2
Critical temperatures of the studied steels. The superscript indicates the heating rate in °C/s.

Steel	A_1, °C	A_1^{10}, °C	A_3, °C	A_3^{10}, °C	A_M, °C
0.2% C	690	713	817	860	870
0.45% C	711	722	770	804	893

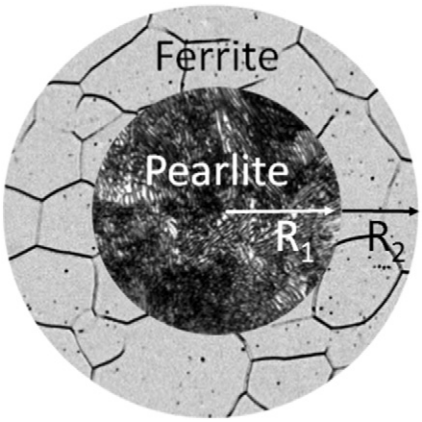

Fig. 1. Scheme of the ferrite-pearlite initial microstructure used to simulate the diffusion-controlled formation of austenite.

3. Results

3.1. Austenite formation at a conventional heating rate

The initial microstructures of both steels are shown in Fig. 2a and e and consist of a mixture of ferrite and pearlite with different volume fractions (Table 4). The microstructural evolution in the samples heated at 10 °C/s to different peak annealing temperatures is shown in Fig. 2b–d and Fig. 2f–h.

Although austenite nucleation sites cannot be identified on the OM images, it is seen that the formation of austenite is quickly consuming the pearlite colonies at 750 °C (Fig. 2b and f).[1] The growth of austenite into pearlite being much faster than into proeutectoid ferrite is based on the absence of pearlite in the heat treated specimens (Fig. 2c, d, g, and h). The rate of the advance of γ/pearlite and γ/α interfaces is also evidenced in the austenite fraction versus temperature curves obtained by dilatometric experiments (Fig. 3). The slope of the experimental dilatometric curves is steep at temperatures below ~750 °C (B_1 lines), where austenite grows mainly into pearlitic grains. This slope decreases with increasing temperature (B_2 lines), when austenite grows into ferrite after pearlite has already been fully consumed.

3.2. Austenite formation under ultrafast heating at 1500 °C/s

The evolution of the microstructure after heating at 1500 °C/s is shown in Fig. 4. Analogous features in the formation of austenite were observed: a very fast transformation of pearlite and a somewhat lower transformation rate at temperatures above 750 °C. Evidence of this pattern is shown in Fig. 3 for heating rates of 450 °C/s and 1500 °C/s. Notice that the austenite volume fractions observed during heating at 450 °C/s and 1500 °C/s are lower compared to those at 10 °C/s at temperatures above 750 °C. The effect of the heating rate on the volume fraction is discussed further in Section 4.2.4.

3.2.1. Nucleation of austenite

The UFH experiments allow the observation of early stages of austenite formation. Nucleation of austenite is observed to take place at α/pearlite and pearlite/pearlite boundaries. Fig. 5a and b illustrate the formation of a nucleus of austenite, which is identified on the basis of

[1] It should be noted that no austenite can be observed on the OM, SEM and TEM images due to its transformation into martensite after quenching.

Table 3
Parameters introduced in the Dictra calculations. f_P is the volume fraction of pearlite.

Steel	R_1, μm	R_2, μm	f_P
0.2% C	10	6.07	0.24
0.45% C	10	1.85	0.60

Table 4
Phase quantification in the initial microstructure (OM based).

Steel	Ferrite fraction [%]	Pearlite fraction [%]	Standard deviation [%]
0.2% C	66.1	33.9	1.3
0.45% C	33.7	66.3	0.7

its morphology, in front of a cementite plate (arrow). Notice that this particular nucleus has formed on a junction between an α/pearlite boundary and a pearlite/pearlite boundary which implies enhanced local energy. Nucleation was also observed within pearlitic colonies, as shown in Fig. 5c and d.

3.2.2. Growth of austenite

Once austenite has nucleated, it grows in all directions. The rate of growth of austenite into pearlite is distinctly higher than the rate of growth into proeutectoid ferrite. The preferential growth of austenite into pearlite, clearly shown in Fig. 6a and b, is direct evidence of its faster kinetics of austenite formation. Consistent with Fig. 3, the transformation of pearlite is the process that influences most the overall kinetics of austenite formation at temperatures up to ~750 °C. At higher temperatures, the kinetics of austenite growth into proeutectoid ferrite is controlling the process.

A clear difference is noticed, however, between the microstructure of samples UFH at 1500 °C/s to ~850 °C and ~900 °C. The ferrite at 850 °C looks similar to the proeutectoid ferrite as shown in Fig. 2a and e, but at 900 °C a microstructural change takes place. The microstructural difference is readily observed for 0.2% C steel in Fig. 4c and d. The SEM images in Fig. 6c and d show in detail the change in ferrite grain size and morphology. The modification in the morphology of ferrite is due to the change in the mechanism of austenite formation.

EBSD maps (cf. Fig. 7) show that the changes in ferrite morphology are taking place as well at a heating rate of 450 °C/s. As defined elsewhere [30], low Image Quality (IQ) areas are associated with martensite, whereas high IQ values represent ferrite. The IQ maps also display similar features as shown in Fig. 2. The grain average IQ values clearly

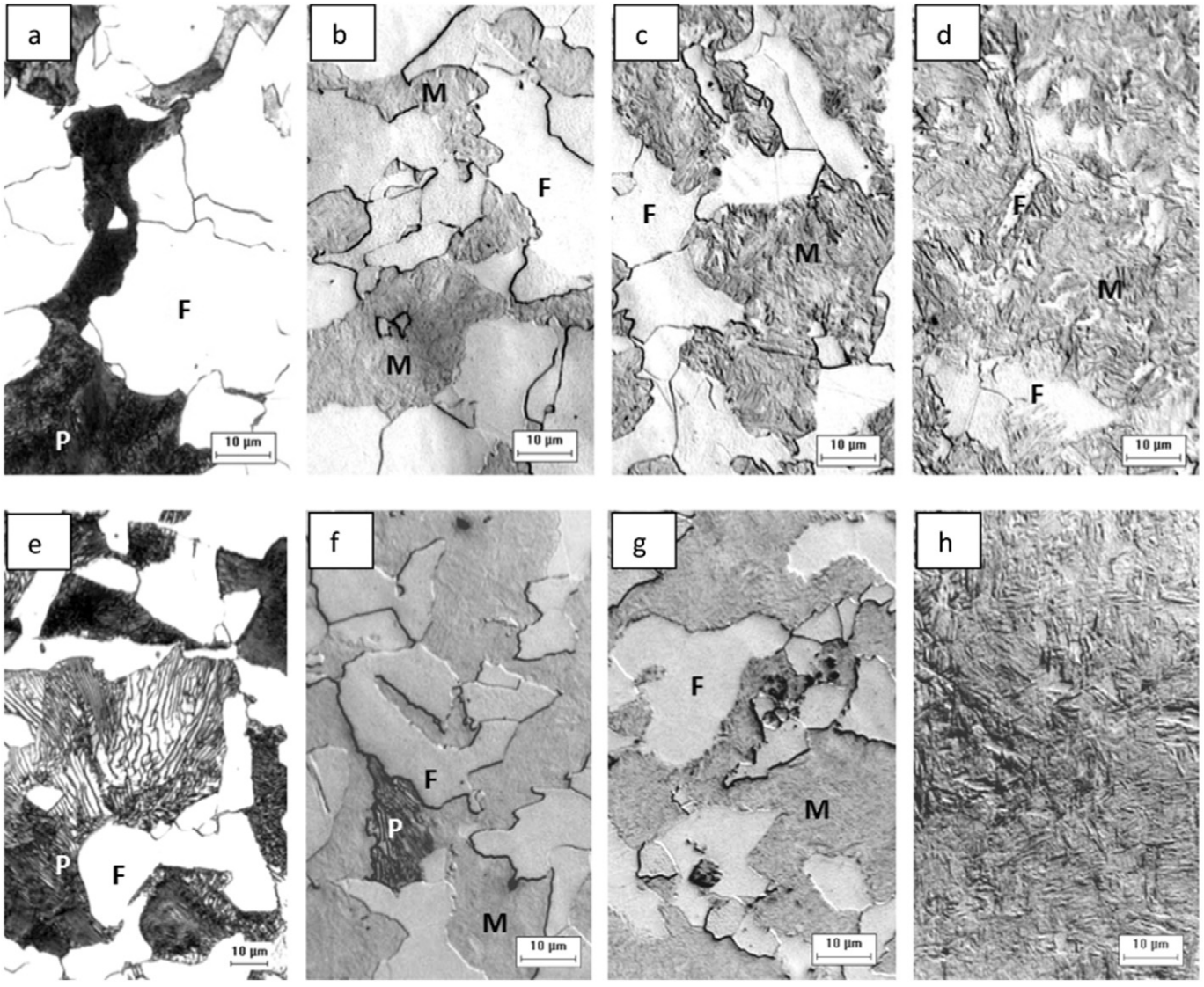

Fig. 2. Microstructure of 0.2% C (a, b, c and d), and 0.45% C (e, f, g and h) heated at 10 °C/s to 750 °C (b, f), 800 °C (c, g) and 850 °C (d, h). (a, b) are images from the initial microstructure. M, P and F correspond to martensite, pearlite and ferrite, respectively. Etched with Nital (4%).

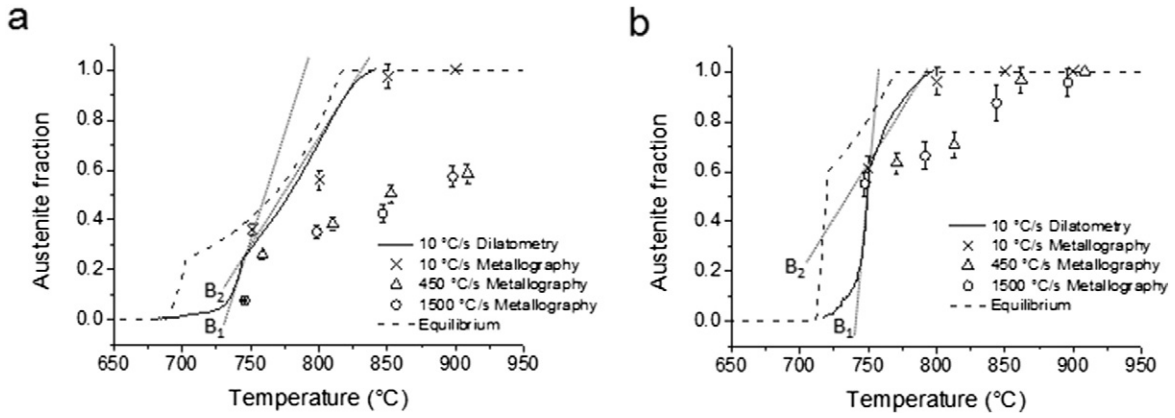

Fig. 3. Austenite fraction (measured as martensite volume fraction) versus temperature for 0.2% C (a) and 0.45% C (b) steels.

show in red-orange the grains of proeutectoid ferrite and in blue-green the grains of martensite. It is clear that the ferrite grains are smaller at 900 °C than at 850 °C. Using the described average IQ criteria, the phase fraction of ferrite was calculated, and information about the equivalent grain diameter was obtained. Table 5 displays the grain diameter of the ferrite after UFH to different peak temperatures. The

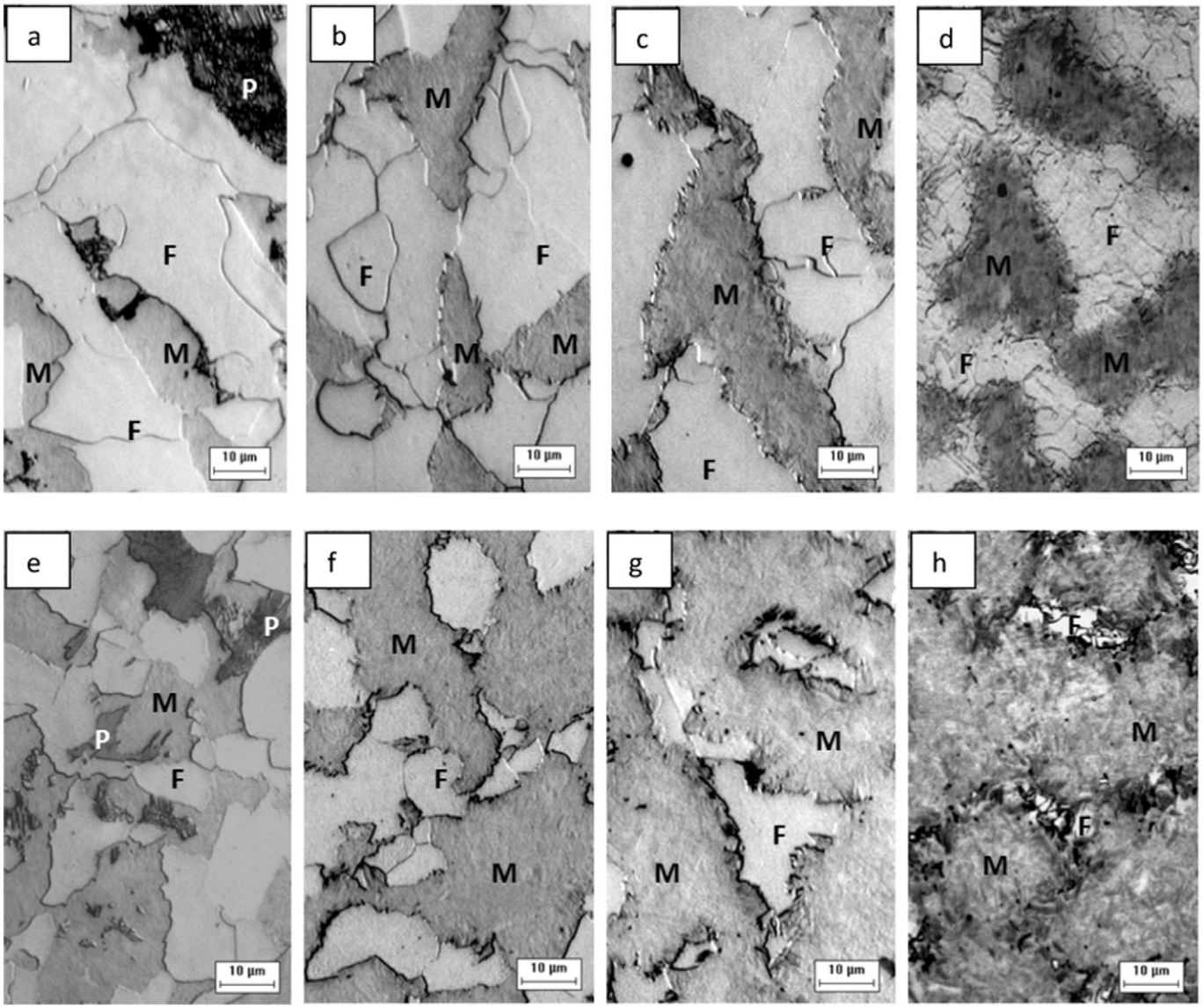

Fig. 4. Microstructure of 0.2% C steel (a, b, c and d), and 0.45% C steel (e, f, g and h) heated at 1500 °C/s to 750 °C (a, e), 800 °C (b, f), 850 °C (c, g) and 900 °C (d, h). M, P and F represent martensite, pearlite and ferrite, respectively. Etched with Nital (4%).

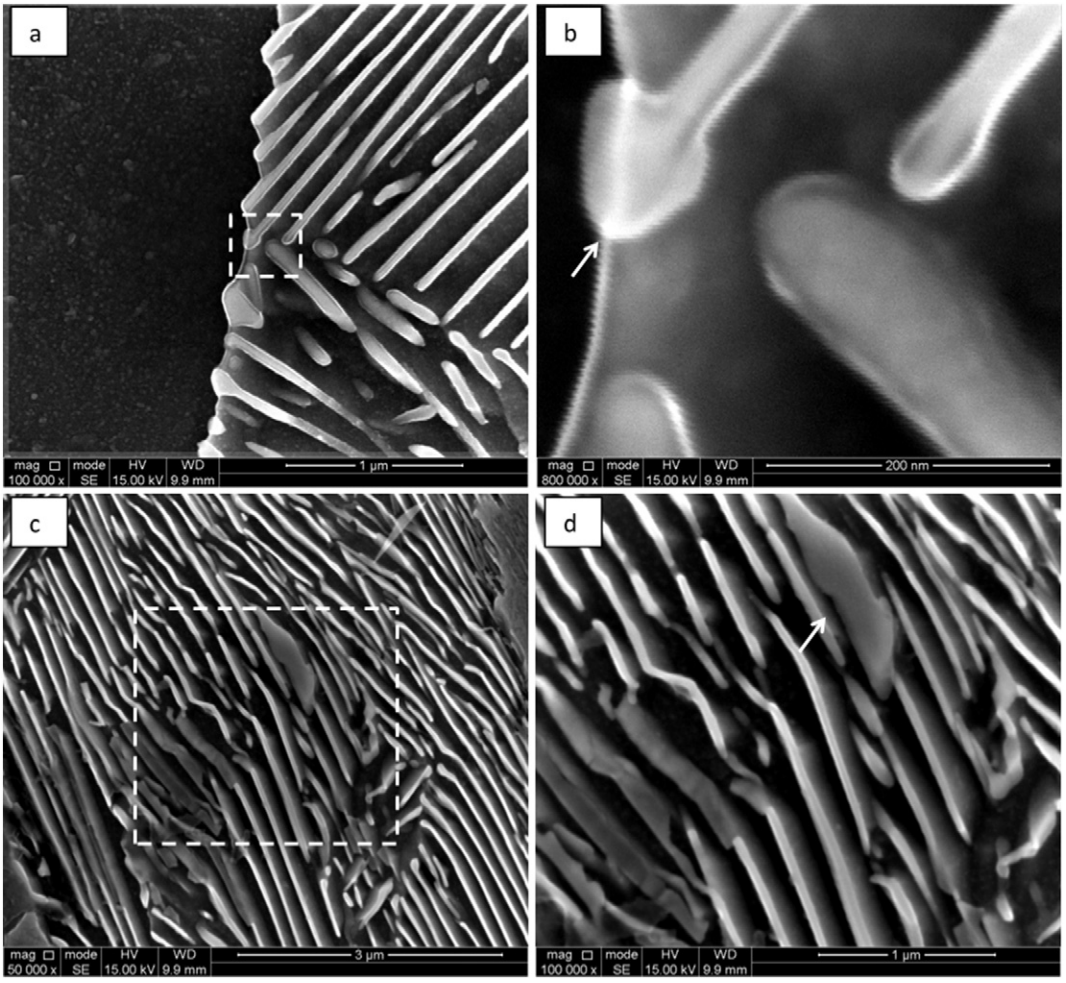

Fig. 5. SEM images of the microstructure of 0.2% C steel heated at 1500 °C/s to 750 °C and quenched. (b) and (d) show the magnified area marked by a white square in (a) and (c), respectively. The white arrow in 5b shows the nucleation of austenite at a junction between a ferrite/pearlite and a pearlite/pearlite boundary, whereas the white arrow in 5d shows the nucleation of austenite inside the pearlitic colony. Etched with Nital (4%).

marked change in the ferritic grain size from 850 °C to 900 °C, qualitatively shown in Fig. 6c, d, and Fig. 7, corresponds to a decrease of around one-half of the original size. This change is not consistent with the decrease in ferritic grain diameter measured from 750 °C to 850 °C (Table 5), and this is believed to be a consequence of a transition in the transformation mechanism of austenite. The transition is further discussed in Section 4.

4. Discussion

4.1. Thermodynamics of austenite formation during anisothermal heating

Microstructural observations indicate that nucleation of austenite is associated with the α/θ interface. When the transformation starts at a certain temperature T in the intercritical range in the Fe-C system, the driving force for the nucleation of austenite is given by the maximum difference between the common tangent between the Gibbs free energy of ferrite in equilibrium with cementite (L_2 in Fig. 8a) and the Gibbs free energy of austenite. The tangent L_2' to the carbon concentration of maximum driving force $X_C^{\gamma,N}$ on the austenite curve has the same slope as L_2, as demonstrated by Hillert [34].

The driving force ξ^N for the nucleation of austenite at the α/θ interface, defined as $\xi^N = -\Delta G$, can be written as

$$\xi^N = \left(\mu_{Fe}^{\alpha/\theta} - \mu_{Fe}^{\gamma,N}\right) = \left(\mu_C^{\alpha/\theta} - \mu_C^{\gamma,N}\right) \quad (1)$$

where $\mu_i^{k/m}$ is the chemical potential of element i in phase k at the k/m interface. The superscript N refers to the nucleation process. This driving force is valid only for nucleation adjacent to a cementite plate, as shown in Fig. 5. Nucleation of austenite at the α/α interface would only take place under the maximum driving force if a fluctuation in the composition of ferrite reaches the value of $X^{\alpha,N}$ (where $X_i^{k/m}$: mole fraction of the element i in phase k at the k/m interface), shown in Fig. 8a. It would thus require diffusion of carbon into ferrite of composition $X^{\alpha/\theta}$ (for the maximum driving force), which is improbable because any compositional change will spontaneously raise the Gibbs free energy of ferrite. Thus, nucleation of austenite at the α/α interface should rarely occur from the thermodynamic point of view.

At the heating rates of the present experiments, the nucleation of austenite always takes place at a temperature in the intercritical range. As the temperature is raised to a certain value T', the austenite becomes more stable, i.e., the free energy curve of austenite will decrease (cf. $G^{\gamma\prime}$, the dashed line in Fig. 8b). It follows that the driving force for nucleation ξ^N will increase. There might be the case when the heating rate is so high that ferrite can transform into austenite of the same chemical composition, i.e., the transformation α → γ will occur for compositions of ferrite for which $G^{\gamma,N} < G^{\alpha/\theta}$ (where $G^{\gamma,N}$ is the Gibbs free energy of austenite nuclei and $G^{\alpha/\theta}$ is the Gibbs free energy of the ferrite in equilibrium with cementite). Under these conditions, nucleation can be accomplished in a massive manner, i.e. without long-range diffusion. The dashed arrow in Fig. 8b represents the driving force for massive formation of austenite from ferrite of composition $X^{\alpha/\theta}$.

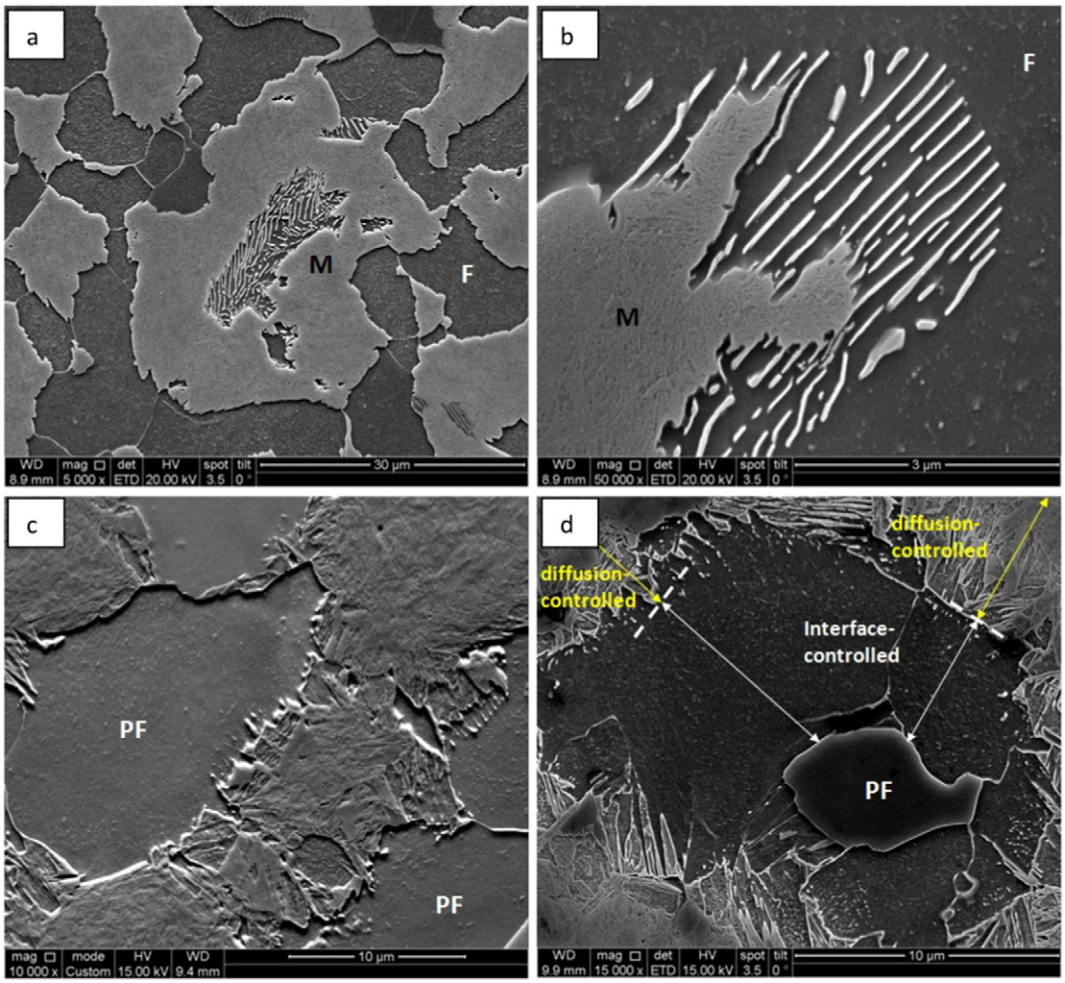

Fig. 6. (a) and (b) Microstructure of the 0.45% C steel heated at 1500 °C/s to 750 °C and quenched, showing the fast advance of austenite into pearlite. (c) and (d) show the microstructure of the 0.2% C steel heated at 1500 °C/s to 850 °C and quenched (c), and 900 °C and quenched (d). A change in the morphology of ferrite is noticed. Arrows in (d) indicate the possible active mechanism during phase transformation. M, F, and PF stand for martensite, ferrite and proeutectoid ferrite. Etched with Nital (4%).

It should be noted, however, that for multicomponent alloys the composition of proeutectoid ferrite and pearlitic ferrite might be significantly different due to the partitioning of substitutional alloying elements and macrosegregation effects. Therefore, massive nucleation of austenite will depend on local chemical conditions and will not be restricted to the α/θ interface.

The growth of austenite takes place towards both pearlite and proeutectoid ferrite. When the austenite nucleated at the α/θ interface begins to grow, the newly formed γ/α interface moves towards both pearlite and proeutectoid ferrite. The derivation for the general case of precipitation from a supersaturated phase under local equilibrium conditions has been developed elsewhere [35]. Austenite at the early stages of its growth is in contact with cementite at one interface and with ferrite on another. This scenario is clearly illustrated in Fig. 5 and Fig. 6. The driving force for austenite growth at the interface with cementite phase is defined by

$$\xi^{\theta\to\gamma} = X_{Fe}^{\gamma/\theta}\left(\mu_{Fe}^{\alpha/\theta} - \mu_{Fe}^{\gamma/\theta}\right) + X_{C}^{\gamma/\theta}\left(\mu_{C}^{\alpha/\theta} - \mu_{C}^{\gamma/\theta}\right) \quad (2)$$

whereas the driving force for austenite growth at the γ/α interface is

$$\xi^{\alpha\to\gamma} = X_{Fe}^{\gamma/\alpha}\left(\mu_{Fe}^{\alpha/\theta} - \mu_{Fe}^{\gamma/\alpha}\right) + X_{C}^{\gamma/\alpha}\left(\mu_{C}^{\alpha/\theta} - \mu_{C}^{\gamma/\alpha}\right) \quad (3)$$

It follows from the local equilibrium conditions that the composition of austenite at the γ/θ interface is different from the composition at the γ/α interface. There will be, therefore, a driving force for carbon diffusion through austenite, defined as $\xi^{D} = \mu_{C}^{\gamma/\theta} - \mu_{C}^{\gamma/\alpha}$. Once the cementite is completely dissolved, diffusion will also smoothen the local fluctuations of carbon in austenite. It should be noted that, similar to the driving force for nucleation, the driving force for carbon diffusion will also increase as the temperature is raised, due to the decrease in the Gibbs free energy of austenite G^{γ} (Fig. 8b), which consequently will decrease $\mu_{C}^{\gamma/\alpha}$ and increase $\mu_{C}^{\gamma/\theta}$.

The growth of austenite during heating at the intercritical range will be controlled by carbon diffusion to the γ/α interface. When the heating rates are low enough, the formation of austenite will be fully accomplished by carbon diffusion and negligible deviations from equilibrium can be expected, as shown in Fig. 3 for 10 °C/s heating rate. When the heating rate is increased, a noticeable deviation from equilibrium fractions is measured. The kinetic nature of the deviation is further discussed in the next section. However, it is important to point out that at ultrafast heating rates (for example, above 450 °C/s for 0.2% C steel as shown in Fig. 3) carbon diffusion does not fully determine the formation rate of austenite. In such case, the system will reach a temperature where austenite will be more stable than ferrite in equilibrium with cementite (cf. arrow Fig. 8b). Schmidt et al. [22] suggested that the temperature T_0, defined as the temperature where $G^{\gamma} = G^{\alpha/\theta}$, is the upper limit for the formation of austenite under carbon diffusion (i.e., the onset of massive formation of austenite). However, such a statement does not apply under local equilibrium conditions. During heating, ferrite in equilibrium with austenite will have chemical

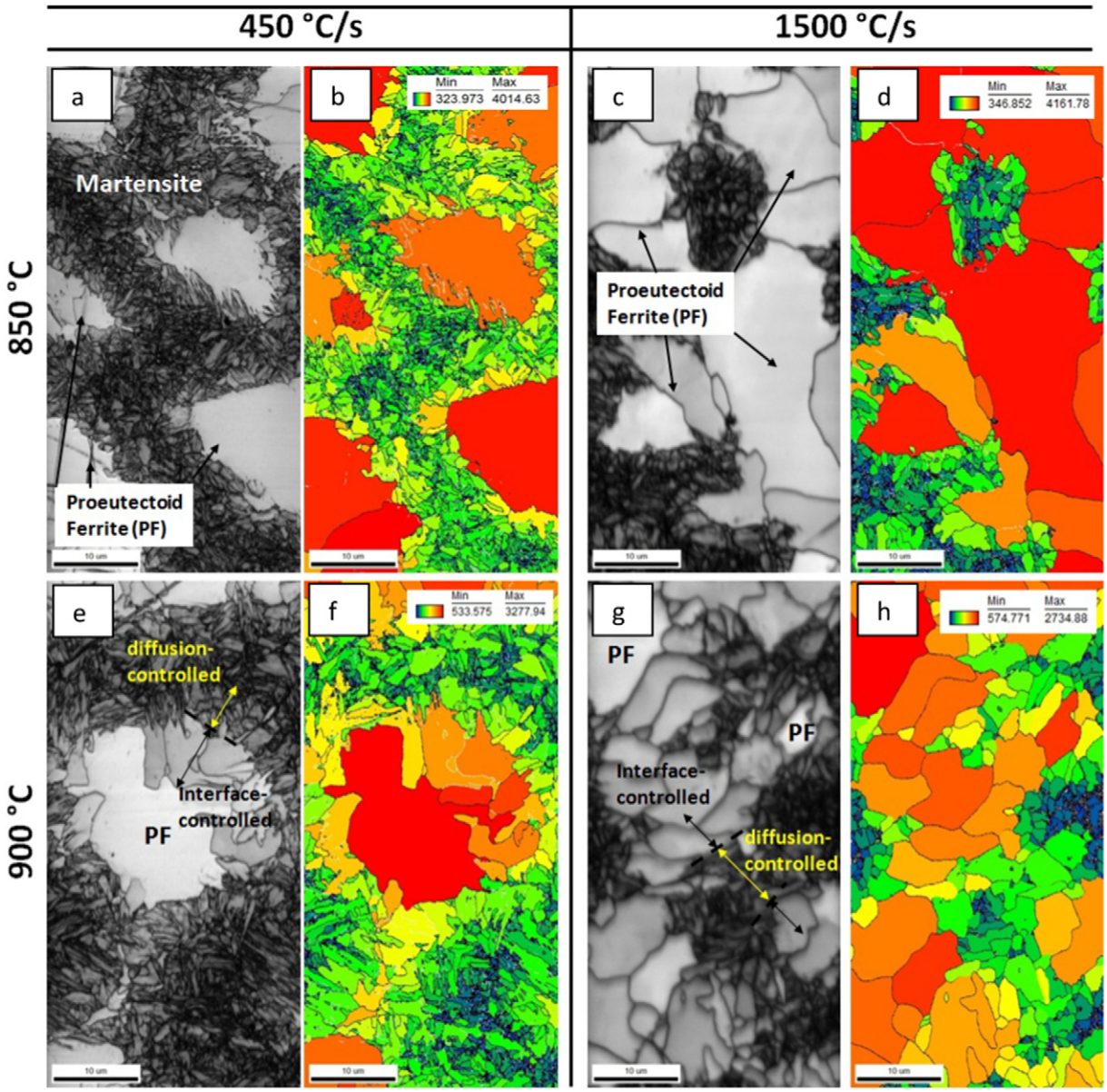

Fig. 7. EBSD images of 0.2% C steel heated to a peak temperature of 850 °C (a, b, c and d) and 900 °C (e, f, g and h). a, b, e and f correspond to a heating rate of 450 °C/s, whereas c, d, g and h to a heating rate of 1500 °C/s. a, c, e and g are Image Quality (IQ) maps and b, d, f and h are grain average IQ (GAIQ) maps. The color bars in b, d, f and h illustrates the intensity of the GAIQ values from the minimum (blue) to the maximum (red), of which the values are indicated in the legends. Arrows in (e) and (g) indicate the possible active mechanisms during phase transformation. Step size 50 nm.

compositions at either side of the interface given by the solvus lines. At a temperature above T_0, as shown by the α/γ tangent L_3 in Fig. 8b, the solvus lines can still be defined by the common tangent and thus carbon diffusion controlled growth of austenite is still the active mechanism. The actual transition to massive formation of austenite will take place at $G^{\gamma} < G^{\alpha}$ when $X_C \rightarrow 0$. The transition temperature will be called A_m, and it has been calculated with ThermoCalc for both steels (Table 2).

Table 5
Average equivalent grain diameter of ferrite at different peak temperatures for heating rates of 450 °C/s and 1500 °C/s. Data calculated from EBSD measurements on 0.2% C steel.

Heating rate, °C/s	Average ferrite grain diameter, μm			
	750 °C	800 °C	850 °C	900 °C
10	18.3	14.9	7.7	–
450	16.2	16.7	13.9	7.56
1500	19.9	20.2	18.7	8.2

The change in the free energy of the system due to the diffusionless transformation of austenite ξ^m is expressed as

$$\xi^m = G^{\alpha} - G^{\gamma} \tag{4}$$

Under continuous heating, the temperature A_m, above which austenite is stable, depends on the local equilibrium conditions at the interface. For pure iron, A_m is given by the allotropic change from α into γ, i.e., 912 °C. Arrows indicate evidence of massive formation of austenite, and subsequent massive transformation of ferrite on cooling, in Fig. 6d and Fig. 7. Proeutectoid ferrite (PF) in Fig. 6c and Fig. 7a, b, c and d shows that the diffusion of carbon controls the advance of the γ/α interface. The morphology of PF grains is analogous to the initial microstructure (Fig. 2a). However, in Fig. 6d and Fig. 7e, f, g and h the morphology and grain size of proeutectoid ferrite have been clearly modified, as described in the previous section. Such changes indicate that a transition of the mechanism of austenite formation from diffusion controlled to

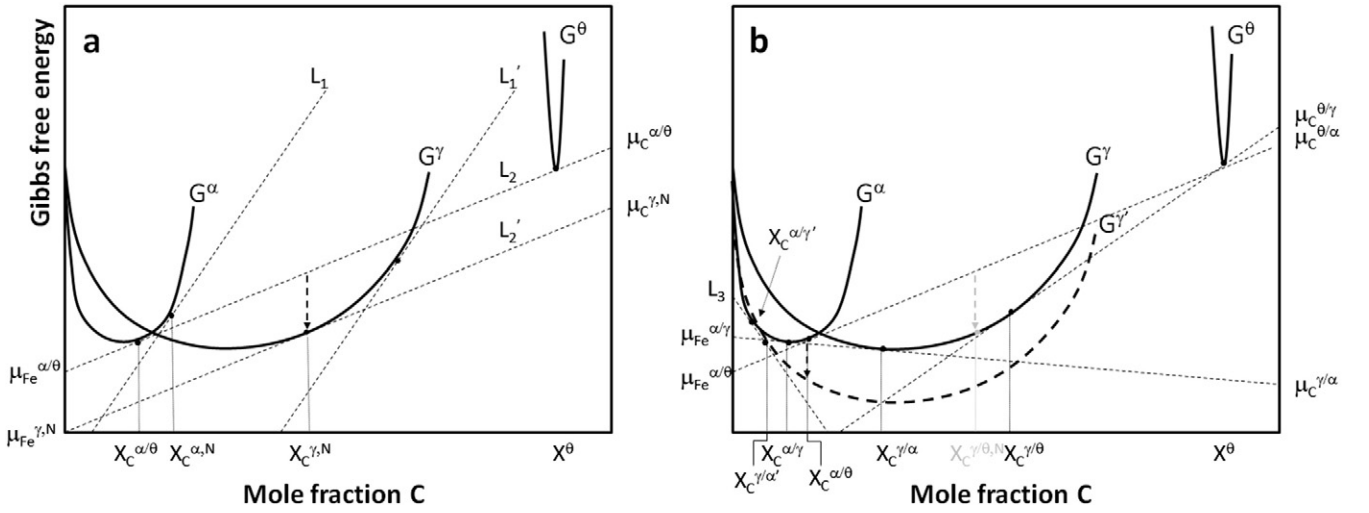

Fig. 8. Gibbs free energy versus composition scheme of (a) the most favorable composition for austenite nucleation from supersaturated ferrite (represented by L_1 and L_1' lines), and from the α/θ interface (represented by L_2 and L_2' lines) for a temperature T above the eutectoid. (b) γ/α and γ/θ equilibrium after nucleation (solid curves) represented by G^α, G^γ, and G^θ at a temperature T above the eutectoid, and the γ/α equilibrium at a temperature T' much above the eutectoid, represented by $G^{\gamma\prime}$ (dashed curve).

interface controlled has taken place, and subsequently, the transformation of ferrite on cooling took place first as interface controlled and then as a diffusion controlled process. The ferrite grain at the center in Fig. 6d suggests that the massive formation of austenite was not complete. It is shown that many different grains of ferrite are surrounding the proeutectoid ferrite, which could be a consequence of several austenite grains formed on heating.

4.2. Kinetics of austenite growth

4.2.1. The mixed-mode model

The mixed-mode model [36] is a sharp interface model which considers that the growth of a new phase from a supersaturated matrix consists of two processes, the diffusion of alloying elements across the interface and the reconfiguration of the atomic structure due to the interface movement. The austenite formation under UFH conditions can be described in the framework of the mixed-mode model. The interface velocity v during the growth of austenite can be defined as

$$v = M \cdot \xi = M\chi \cdot \left(X_C^{\gamma} - X_C^{\gamma\prime}\right) \tag{5.1}$$

where M is the mobility of the γ/α interface, χ a proportionality constant, X_C^{γ} is the composition of the carbon-rich austenite and $X_C^{\gamma\prime}$ is the composition of austenite at the γ/α interface. The mixed nature of the transformation kinetics is estimated by the introduction of the parameter S to the previous expression when relating to the maximum driving force $\chi \cdot (X_C^{\gamma} - X_C^{\gamma/\alpha})$:

$$v = M\chi \cdot S\left(X_C^{\gamma} - X_C^{\gamma/\alpha}\right) \tag{5.2}$$

The parameter S in the kinetic model for the austenite formation can be interpreted as the fraction of the available driving force consumed solely by the movement of the interface. It also indicates the two extreme cases. When $S \to 0$ carbon diffusion controls the advance of the interface. This is a consequence of the mobility M being relatively high. The formation of austenite at low temperatures in the intercritical range (low S values) is very slow due to the diffusion of carbon [37]. When $S \to 1$ the phase transformation is controlled by the interface mobility, which becomes low. The intermediate case, represented by values of S between 0 and 1, takes place when both diffusion and the interface movement are dissipating the available driving force for the formation of austenite. The diffusion of carbon becomes faster than the mobility as the temperature is raised, thus it is reasonable to expect that the formation of austenite will gradually approach an interface control mode, as predicted by the values of the parameter S at high temperatures. The mixed-mode model provides an overall picture of the kinetics of austenite formation during heating. In the next sections, the formation of austenite will be adapted to the specific initial microstructure and the effect of the heating rate will be described.

4.2.2. Diffusion controlled growth of austenite

As stated in the previous section, the austenite nucleates preferentially at the α/θ interfaces, and it subsequently grows into pearlite and proeutectoid ferrite. However, the kinetics of austenite growth is different depending on whether it grows into pearlite or proeutectoid ferrite. A mass balance proposed initially by Brandt [38] led Speich and Richards [39] to derive a kinetic expression for the velocity of isothermal growth of austenite into pearlite. Hillert [3] has obtained a similar relation which also takes into account the diffusion of carbon in ferrite. We employ the equation by Hillert [3], rewritten as

$$v^{\gamma \to P} = \frac{D_C^{\gamma}\left(X_C^{\gamma/\theta} - X_C^{\gamma/\alpha}\right) - D_C^{\alpha}\left(X_C^{\alpha/\gamma} - X_C^{\alpha/\theta}\right)}{S_P\left(X_C^{\gamma/\alpha} - X_C^{\alpha}\right)} \tag{5.3}$$

where $v^{\gamma \to P}$ is the velocity of the γ/α interface moving towards pearlite, D_i^k is the diffusion coefficient for the element i in the phase k, and S_P the pearlitic interlamellar spacing. Notice that volume changes are neglected. The advance of the austenite into the proeutectoid ferrite can be approximated by a mass-balance construction similar to what has been previously proposed by Zener [40] and is given by

$$v^{\gamma \to \alpha} = \frac{D_C^{\gamma}\left(X_C^{\gamma} - X_C^{\gamma/\alpha}\right)}{L\left(X_C^{\gamma/\alpha} - X_C^{\alpha/\gamma}\right)} \tag{6}$$

where $v^{\gamma \to \alpha}$ is the velocity of the γ/α interface moving towards proeutectoid ferrite, X_C^{γ} is the composition of the carbon-rich austenite and L can be regarded as the effective diffusion distance in austenite. It is clear from Eq. (6) that the growth will stop when the carbon in austenite is homogeneously distributed, i.e., $X_C^{\gamma} = X_C^{\gamma/\alpha}$. The diffusion distance S_P (interlamellar spacing) in Eq. (5.3) can be expected to be one or two orders of magnitude smaller than L (on the order of one-half of the size of the pearlite colony) in Eq. (6). One might thus reasonably suggest that the growth of austenite towards pearlite will be faster

than the growth of austenite into proeutectoid ferrite. It has been reported elsewhere [27], for a heating rate of 20 °C/s, that experimental interface velocities can be around two times higher for austenite growing into pearlite, compared to austenite growing into ferrite. Similar results are found also in this work (see Section 3.1, Fig. 3).

4.2.3. Massive growth of austenite

As described in the previous section, the formation of austenite could proceed in a diffusionless way in UFH experiments when $\Delta G^{m} < 0$. A kinetic expression for the γ/α interface velocity is

$$v^m = M \cdot \xi^m = -M \cdot \Delta G$$

where v^m is the velocity of the γ/α interface formed by a massive mechanism and M the mobility of the γ/α interface. Essentially there are no differences in mobility of the γ/α interface at temperatures below and above A_m. The only difference is that above A_m there is no driving force to be dissipated by diffusion [41].

Evidence of massive formation of austenite is shown in Fig. 4d, Fig. 6d and Fig. 7e. Fig. 6d also illustrates several transformation products formed on cooling. The mixture of microconstituents is a consequence of the carbon gradients in austenite. Such transformation products have been reported elsewhere [42] for UFH experiments. In the same way, the points corresponding to heating rates of 450 °C/s and 1500 °C/s above A_m in Fig. 3a represent the fraction of martensite formed on cooling. The data mentioned above does not represent the fraction of austenite because a significant fraction was formed massively during heating, and subsequently was transformed back into ferrite under the same mechanism. The points above A_m for heating rates of 450 °C/s and 1500 °C/s measured in Fig. 3a are therefore related to the position of the carbon diffusion front in austenite (cf. dashed line in Fig. 6d) and not to the actual fraction of austenite on heating.

4.2.4. Dictra calculations

Simulations of austenite growth into proeutectoid ferrite at different heating rates were carried out using Dictra. The plots of the simulated austenite fraction versus temperature and simulated interface velocity versus temperature in Fig. 9 can be interpreted with reference to Eq. (6). Fig. 9a and b show the phase fractions of austenite formed during heating at 10 °C/s, 450 °C/s and 1500 °C/s. When the heating rate is increased, the slope of the curve gradually decreases. These theoretical results are in very good agreement with experimental observations of austenite formation from ferrite-pearlite aggregates at different heating rates reported earlier in the literature [25] and also with our experimental observations (Section 3.1, Fig. 3).

The change in the slope of the phase volume fraction curve can be estimated by proposing the following variable

$$\beta = \frac{dT}{dt} \tag{7}$$

where β is the heating rate, T temperature and t time.

Further integration in Eq. (6) will produce an expression that relates distance and temperature multiplied by a factor $^{1}/_{\beta}$. For a spherical

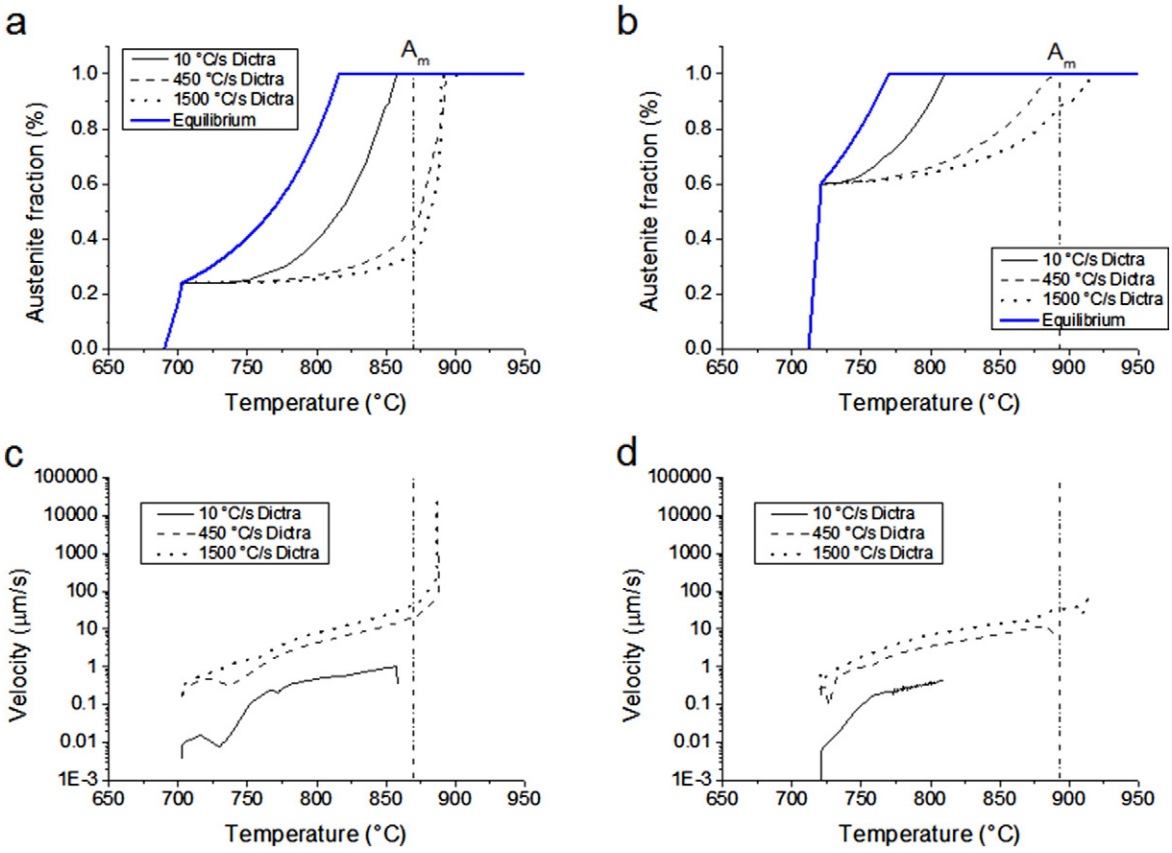

Fig. 9. Dictra calculations of the austenite fraction formed on heating at different heating rates versus temperature (a, b) and the velocity of the γ/α interface at different heating rates versus temperature (c, d). (a, c) were calculated for 0.20% C steel and (b, d) for 0.45% C steel. A_m (dashed-dotted line) represents the lowest temperature of the fully austenitic range (see Table 2).

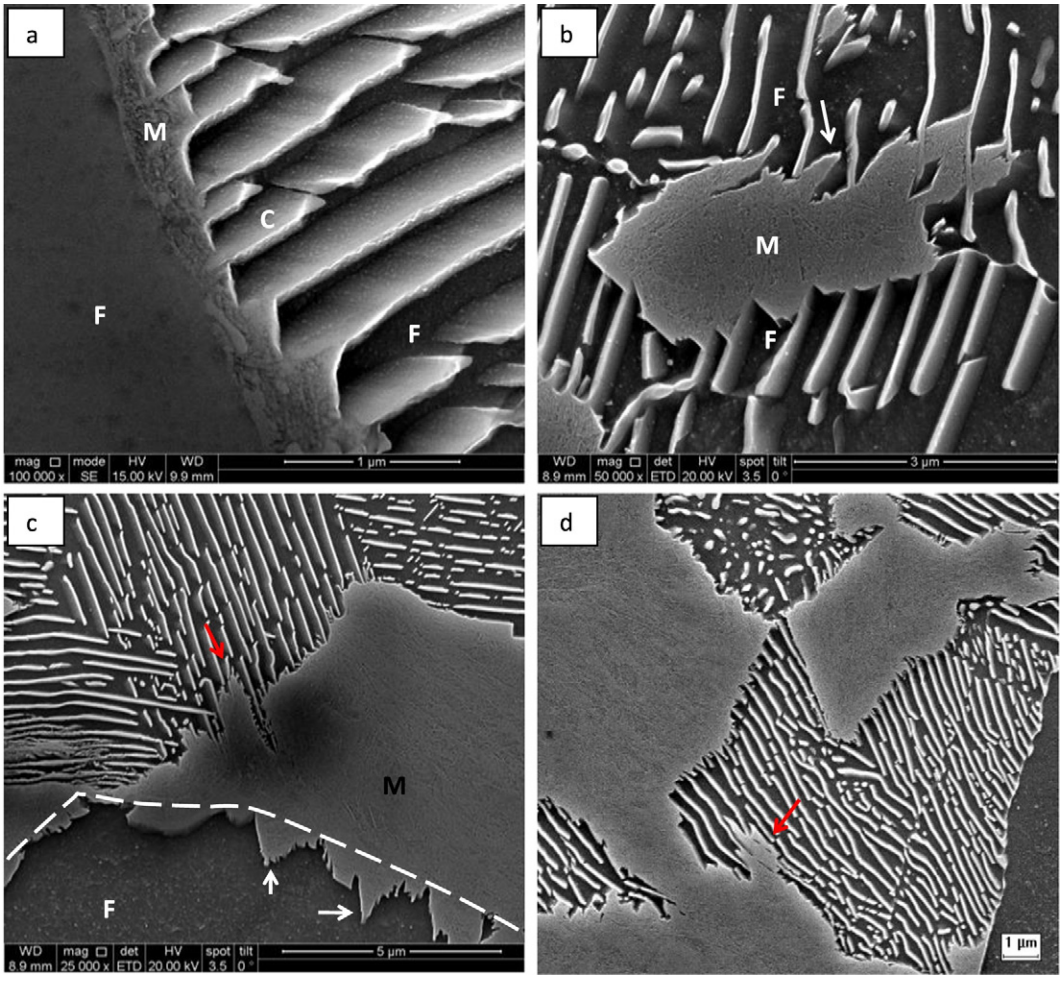

Fig. 10. Microstructure of 0.2% C (a) and 0.45% C (b, c, and d) steels heated at 1500 °C/s to 750 °C and quenched, illustrating the growth of austenite with different interface morphologies. M, F and C stand for martensite, cementite and ferrite. Etched with Nital (4%).

geometry, as in the Dictra calculations, the volume fraction can be computed as

$$v^{\gamma\to\alpha} = \frac{dr}{dt} = \beta\frac{dr}{dT} = \beta\cdot v(T)^{\gamma\to\alpha}$$
$$v(T)^{\gamma\to\alpha} = \frac{1}{\beta}\cdot\frac{dr}{dt} = \frac{1}{\beta}\cdot\frac{D_C^{\gamma}\left(X_C^{\gamma}-X_C^{\gamma/\alpha}\right)}{L\left(X_C^{\gamma/\alpha}-X_C^{\alpha/\gamma}\right)} \quad (8)$$

$$f = \frac{r_T^3}{r_0^3} \quad (9)$$

where $v^{\gamma\to\alpha}$ is the velocity of the interface as a function of temperature, f is the phase fraction of austenite as a function of temperature, r_0 the radius of the volume and r_T the position of the γ/α interface at temperature T and heating rate β. As the heating rate is increased, one should expect a smaller fraction of austenite for a given temperature, or a displacement in the curve towards higher temperatures, as shown in Fig. 9a and b.

Fig. 9c and d show that the velocity of the γ/α interface increases as the heating rate is elevated. Such an increase can also be rationalized based on Eq. (6). At low heating rates, the value of $X_C^{\gamma} - X_C^{\gamma/\alpha}$ is smaller compared to values for high heating rates because the differences in carbon concentration in austenite have more time to relax at low heating rates. At high heating rates, the value of $X_C^{\gamma} - X_C^{\gamma/\alpha}$ will be larger, and the carbon gradient in austenite will be steeper, thereby increasing the γ/α interface velocity. In a previous study [42], the effect of heating rate on the formation of carbon gradients in austenite has been developed, and consistent calculations have been introduced. It is also remarkable that the velocities shown in Fig. 9c and d are virtually the same for 0.2% C and 0.45% C steels in the temperature range from the onset of austenite formation up to A_m. Such results show that the relative volume fractions of the ferrite-pearlite aggregate do not influence the mobility of the advancing interface nor its driving force significantly. Hence the simplified model described in Eq. (6), which mainly accounts for the interface conditions of the moving boundary, is a suitable representation for the diffusion controlled growth of austenite.

In addition to the elevated value of D_C^{γ}, the factor $X_C^{\gamma/\alpha} - X_C^{\alpha/\gamma}$ becomes very small at temperatures close to A_m for heating rates higher than 450 °C/s, and thus the predicted interface velocity achieves very high values, unrealistic for austenite formation processes. It should be noted that Dictra only performs calculations under conditions of infinite interface mobility ($S \to 0$ for the mixed-mode model). Fig. 9c shows very steep calculated interface velocities at temperatures above A_m, which do not correspond to the actual kinetics of γ/α interface formation. As stated in Sections 4.1 and 4.2.1, the formation of austenite above A_m is interface controlled, and its kinetics are governed by the mobility of the interface and the available driving force. Dictra, therefore, significantly overestimates the transformation rate because of the assumption of infinite interface mobility. The actual onset of the massive formation of austenite, i.e. A_m, is thus proposed as the temperature where the Gibbs free energy of austenite G^{γ} becomes lower than the Gibbs free

energy of ferrite G^{α} when $X_C \rightarrow 0$. However, a significant partitioning of alloying elements in pearlite and proeutectoid ferrite is to be expected in the initial microstructures. Thus, the variations in the Gibbs free energy curves and hence in the interface equilibrium conditions within the microstructure need to be considered for a reasonable thermodynamic and kinetic description of austenite formation.

4.2.5. Morphologies of the γ/α interface

At the initial stages of austenite formation, the γ/α interface in most cases is planar. However, in some cases, the shape of the interface is acicular, irrespective of its advance towards pearlite or proeutectoid ferrite. Both cases are clearly shown in Fig. 10. Fig. 10a shows the case of the planar γ/α interface growing towards proeutectoid ferrite and Fig. 10b shows the lower side of the austenite grain growing into pearlite. Meshkov and Pereloma [17] reported planar γ/α interfaces moving into pearlite in fast heating experiments, yet the acicular austenite growing into pearlite has not been observed. White arrows show Widmanstätten austenite in Fig. 10b in a very early stage advancing towards pearlite (upper side) and also in Fig. 10c moving into proeutectoid ferrite. In some cases, a different kind of non-planar advance of the γ/α interface in pearlite was observed, as shown by the red arrows in Fig. 10c and d. It is not clear whether this particular interface morphology corresponds to a Widmanstätten plate or to another possible feature, like nucleation of austenite (as shown in Fig. 5d) just in front of the moving boundary.

The red arrow in Fig. 10d illustrates a zone similar to that which is marked by the red arrow in Fig. 10c. In this case, the austenite has developed a flat interface with pearlite in almost all fronts, except in the area previously mentioned. Similar to Fig. 5d, the morphology ahead the γ/α front, marked by the red arrow in Fig. 10d, suggests the nucleation of austenite (martensite). Martensite lies in seemingly unconnected areas, which suggests different nucleation sites for austenite. It was previously stated that the driving force for nucleation of austenite increases as the heating rate is raised. Thus, one can expect that the nucleation might be spontaneously activated within pearlite in a continuous heating experiment at UFH rates and hence produces the morphologies at the γ/α interface as shown in Fig. 10c and Fig. 10d. Such morphologies of the γ/α interface have not been reported previously in isothermal experiments, probably due to the very fast growth of austenite into pearlite at the comparatively low heating rates resulting in a rapid full consumption of pearlite by growing austenite. It is also reasonable to suggest a continuous nucleation regime for the formation of austenite towards pearlite for UFH heating experiments.

5. Conclusions

The effect of conventional (10 °C/s), fast (50 °C/s–100 °C/s) and ultrafast heating rates (higher than 100 °C/s) on the austenite nucleation and growth is studied experimentally and theoretically in 0.2% C and 0.45% C steels with initial ferrite-pearlite microstructure. The main findings of this work include:

1. Austenite nucleation occurs preferably at the α/pearlite interfaces. As discussed in Section 4.1, ultrafast heating might substantially increase the driving force for austenite nucleation, and thereby its chances of formation at the less favorable α/θ interfaces. The newly formed austenite grows in all directions, though its growth rate into pearlite is higher compared to the growth rate into proeutectoid ferrite. It is experimentally demonstrated for the first time that possible nucleation of austenite ahead of the γ/α interface significantly modifies the shape of the boundary moving through pearlite.
2. Carbon diffusion governs austenite formation and growth during heating with conventional heating rates. In ultrafast heating regimes, this mechanism is responsible for the growth at the early stages of austenite formation and then a massive mechanism replaces it. This transition occurs at the so-called A_m temperature which is defined thermodynamically.
3. A simplified kinetic description of the austenite formation is provided. The local chemical composition at the γ/α interface determines the velocity of the moving boundaries below A_m. The kinetic description shows that the heating rate has a considerable impact on the relaxation of carbon concentration gradients in austenite and thus on the interface velocity. There is essentially no difference in the velocity of γ/α interface moving towards proeutectoid ferrite between 0.2% C and 0.45% C steels of ferrite-pearlite initial microstructure below A_m.

Acknowledgements

The CONICYT-PCHA/Doctorado Nacional/2013 Ph.D. scholarship for F. Castro Cerda is gratefully acknowledged. Authors appreciate the comments of V. Bliznuk from Ghent University. I. Sabirov acknowledges the Spanish Ministry of Economy and Competitiveness for financial support through the Ramon y Cajal Fellowship (RYC-2011-08881).

References

[1] R.F. Mehl, The mechanism and rate formation of austenite from ferrite-cementite aggregates, Trans. ASM. 31 (1943) 613–650.
[2] G.R. Speich, A. Szirmae, Formation of austenite from ferrite and ferrite-carbide aggregates, Trans. AIME 245 (1969) 1063–1073.
[3] M. Hillert, K. Nilsson, L.-E. Torndahl, Effect of alloying elements on the formation of austenite and dissolution of cementite, J. Iron Steel Inst. 49–66 (1971).
[4] Y. Gu, P. Tian, X. Wang, X. Han, B. Liao, F. Xiao, Non-isothermal prior austenite grain growth of a high-Nb {X100} pipeline steel during a simulated welding heat cycle process, Mater. Des. 89 (2016) 589–596, http://dx.doi.org/10.1016/j.matdes.2015.09.039.
[5] W.I. Haworth, J.G. Parr, The effect of rapid heating on the alpha-gamma transformation of iron, Trans. ASM. 58 (1965) 476–488.
[6] R.R. Judd, H.W. Paxton, Kinetics of austenite formation from a spheroidized ferrite-carbide aggregate, Trans. AIME 242 (1968) 206–215.
[7] V.N. Gridnev, V.I. Trefilov, Over the reversability of the martensitic transformation in Fe-C alloys during heating, Dokl. Akad. Nauk SSSR 95 (1954) 741–743.
[8] T. Garcin, K. Ueda, M. Militzer, Reverse austenite transformation and grain growth in a low-carbon steel, Metall. Mater. Trans. A. 1–13 (2016)http://dx.doi.org/10.1007/s11661-016-3855-2.
[9] E. López-Martínez, O. Vázquez-Gómez, H.J. Vergara-Hernández, B. Campillo, Effect of initial microstructure on austenite formation kinetics in high-strength experimental microalloyed steels, Int. J. Miner. Metall. Mater. 22 (2015) 1304–1312, http://dx.doi.org/10.1007/s12613-015-1198-4.
[10] D. Xu, Y. Liu, J. Li, Q. Meng, P. Li, Microstructure characterization and mechanical properties of TRIP-aided steel under rapid heating for different holding time, J. Iron Steel Res. Int. 23 (2016) 138–144, http://dx.doi.org/10.1016/S1006-706X(16)30025-5.
[11] N. Li, J. Lin, D.S. Balint, T.A. Dean, Modelling of austenite formation during heating in boron steel hot stamping processes, J. Mater. Process. Technol. 237 (2016) 394–401, http://dx.doi.org/10.1016/j.jmatprotec.2016.06.006.
[12] P. Li, J. Li, Q. Meng, W. Hu, D. Xu, Effect of heating rate on ferrite recrystallization and austenite formation of cold-roll dual phase steel, J. Alloys Compd. 578 (2013) 320–327, http://dx.doi.org/10.1016/j.jallcom.2013.05.226.
[13] S. Sharma, T. Nanda, M. Adhikary, T. V., B. R.K., A simulation study of pearlite-to-austenite transformation kinetics in rapidly heated hot-rolled low carbon steel, Mater. Des. 107 (2016) 65–73, http://dx.doi.org/10.1016/j.matdes.2016.06.025.
[14] Q. Meng, J. Li, H. Zheng, High-efficiency fast-heating annealing of a cold-rolled dual-phase steel, Mater. Des. 58 (2014) 194–197, http://dx.doi.org/10.1016/j.matdes.2014.01.055.
[15] F. Cordovilla, Á. García-Beltrán, P. Sancho, J. Domínguez, L. Ruiz-de-Lara, J.L. Ocaña, Numerical/experimental analysis of the laser surface hardening with overlapped tracks to design the configuration of the process for Cr-Mo steels, Mater. Des. 102 (2016) 225–237, http://dx.doi.org/10.1016/j.matdes.2016.04.038.
[16] N. Li, J. Lin, D.S. Balint, T.A. Dean, Experimental characterisation of the effects of thermal conditions on austenite formation for hot stamping of boron steel, J. Mater. Process. Technol. 231 (2016) 254–264, http://dx.doi.org/10.1016/j.jmatprotec.2015.12.008.
[17] Y.Y. Meshkov, E.V. Pereloma, Phase Transformations in Steels, Elsevier, 2012http://dx.doi.org/10.1533/9780857096104.4.581.
[18] W.J. Kaluba, R. Taillard, J. Foct, The bainitic mechanism of austenite formation during rapid heating, Acta Mater. 46 (1998) 5917–5927.
[19] H.I. Aaronson, J.F. Nie, Discussion to "The bainitic mechanism of austenite formation during rapid heating", Scr. Mater. 42 (1998) 505–509.
[20] M. Hillert, Comments on "The bainite mechanism of austenite formation during rapid heating", Scr. Mater. 43 (2000) 1045–1046.
[21] W.J. Kaluba, R. Taillard, J. Foct, Reply to 'comments on "the bainitic mechanism of austenite formation during rapid heating"', Scr. Mater. 43 (2000) 1047–1049, http://dx.doi.org/10.1016/S1359-6462(00)00533-9.
[22] E.D. Schmidt, E.B. Damm, S. Sridhar, A study of diffusion- and interface-controlled migration of the Austenite/Ferrite front during Austenitization of a case-hardenable

alloy steel, Metall. Mater. Trans. A Phys. Metall. Mater. Sci. 38 (2007) 698–715, http://dx.doi.org/10.1007/s11661-007-9208-4.
[23] V.I. Savran, S.E. Offerman, J. Sietsma, Austenite nucleation and growth observed on the level of individual grains by three-dimensional X-ray diffraction microscopy, Metall. Mater. Trans. A. 41 (2010) 583–591, http://dx.doi.org/10.1007/s11661-009-0142-5.
[24] J. Rödel, H.J. Spies, Modelling of austenite formation during rapid heating, Surf. Eng. 12 (1996) 8–13.
[25] R.C. Dykhuizen, C.V. Robino, G.A. Knorovsky, A method for extracting phase change kinetics from dilatation for multistep transformations: austenitization of a low carbon steel, Metall. Mater. Trans. B. 30 (1999) 107–117, http://dx.doi.org/10.1007/s11663-999-0011-z.
[26] A.I. Katsamas, A computational study of austenite formation kinetics in rapidly heated steels, Surf. Coat. Technol. 201 (2007) 6414–6422, http://dx.doi.org/10.1016/j.surfcoat.2006.12.014.
[27] E. Schmidt, Y. Wang, S. Sridhar, A study of nonisothermal austenite formation and decomposition in Fe-C-Mn alloys, Metall. Mater. Trans. A. 37A (2006) 1799–1810, http://dx.doi.org/10.1007/s11661-006-0122-y.
[28] T.A. Kop, Dilatometric Study of the Austenite/Ferrite Interface Mobility(Ph. D. Thesis) TU Delft, 2000.
[29] V.I. Savran, Austenite Formation in C-Mn Steel(Ph. D. Thesis) TU Delft, 2009.
[30] R.H. Petrov, L.A.I. Kestens, Advanced high-strength steels: electron backscatter diffraction (EBSD), in: R. Colás, G.E. Totten (Eds.), Encycl. Iron, Steel, Their Alloy, CRC Press 2016, pp. 46–69, http://dx.doi.org/10.1081/E-EISA-120050786.
[31] J.-O. Andersson, L. Höglund, B. Jönsson, J. Ågren, Fundamentals and Applications of Ternary Diffusion, Elsevier, 1990, http://dx.doi.org/10.1016/B978-0-08-040412-7.50023-2.
[32] A. Borgenstam, L. Höglund, J. Ågren, A. Engström, DICTRA, a tool for simulation of diffusional transformations in alloys, J. Phase Equilibria. 21 (2000) 269–280, http://dx.doi.org/10.1361/105497100770340057.
[33] J.-O. Andersson, T. Helander, L. Höglund, P. Shi, B. Sundman, Thermo-Calc & DICTRA, computational tools for materials science, Calphad 26 (2002) 273–312, http://dx.doi.org/10.1016/S0364-5916(02)00037-8.
[34] M. Hillert, Nuclear composition—a factor of interest in nucleation, Acta Metall. 1 (1953) 764–766, http://dx.doi.org/10.1016/0001-6160(53)90043-1.
[35] M. Hillert, The uses of free energy-composition diagrams, in: H.I. Aaronson (Ed.), Lect. Theory Phase Transform, Metallurgical Society of AIME 1975, pp. 1–50.
[36] J. Sietsma, S. van der Zwaag, A concise model for mixed-mode phase transformations in the solid state, Acta Mater. 52 (2004) 4143–4152, http://dx.doi.org/10.1016/j.actamat.2004.05.027.
[37] G.R. Speich, V.A. Demarest, R.L. Miller, Formation of austenite during intercritical annealing of dual-phase steels, Metall. Trans. A. 12 (1981) 1419–1428, http://dx.doi.org/10.1007/BF02643686.
[38] W.H. Brandt, Solution of the diffusion equation applicable to the edgewise growth of pearlite, J. Appl. Phys. 16 (1945) 139–146, http://dx.doi.org/10.1063/1.1707565.
[39] G.R. Speich, M.J. Richards, Appendix - diffusion equations for pearlite dissolution, Trans. AIME 245 (1969) 1073–1074.
[40] C. Zener, Theory of growth of spherical precipitates from solid solution, J. Appl. Phys. 20 (1949) 950–953, http://dx.doi.org/10.1063/1.1698258.
[41] M. Hillert, Solute drag, solute trapping and diffusional dissipation of Gibbs energy, Acta Mater. 47 (1999) 4481–4505, http://dx.doi.org/10.1016/S1359-6454(99)00336-5.
[42] F.M. Castro Cerda, C. Goulas, I. Sabirov, S. Papaefthymiou, A. Monsalve, R.H. Petrov, Microstructure, texture and mechanical properties in a low carbon steel after ultra-fast heating, Mater. Sci. Eng. A 672 (2016) 108–120, http://dx.doi.org/10.1016/j.msea.2016.06.056.